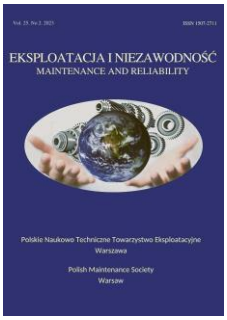

Eksploatacja i Niezawodnosc – Maintenance and Reliability

Volume 28 (2026), Issue 4

journal homepage: http://www.ein.org.pl

Article citation info:
Wei L, Wu Q, Song Y, Wang H, Novel composite label driven improved GAN for high fidelity bearing fault diagnosis under variable and imbalanced conditions, Eksploatacja i Niezawodnosc – Maintenance and Reliability 2026: 28(4) http://doi.org/10.17531/ein/220208

Novel composite label driven improved GAN for high fidelity bearing fault diagnosis under variable and imbalanced conditions

Indexed by: Web of Science Group

Lunpan Wei[a], Qilong Wu[a], Yanjie Song[b], He Wang[c,*]

[a] School of Electronic Engineering, Huainan Normal University, China
[b] School of Information Science and Technology, Dalian Maritime University, China
[c] College of Intelligent Science and Engineering, Harbin Engineering University, China

Highlights

- Proposes a 5D Composite Label Vector for physical control.
- Improved GAN uses conditional injection & Asymmetric Learning Rates.
- Generated high-fidelity data boosts accuracy and noise robustness.
- Model synthesizes fault data for unseen operating conditions.

Abstract

Rolling bearing fault diagnosis faces severe challenges from data imbalance and variable operating conditions, restricting model generalization. We propose an Improved Generative Adversarial Network (IGAN) for high-fidelity fault sample synthesis. Core innovations are: 1) A 5-dimensional Composite Label Vector (CLV) that encodes physical information (load, fault diameter, location); 2) A robust conditional injection mechanism mapping labels to a high-dimensional space for precise guidance; 3) An Asymmetric Learning Rate (ALR) strategy for training stability. Comparative experiments on the CWRU dataset demonstrate that the proposed IGAN outperforms state-of-the-art baselines, boosting classifier accuracy to 99.1%. More importantly, the model synthesizes high-fidelity data for entirely unseen operating conditions via label vector interpolation and demonstrates strong generalization on the IMS natural run-to-failure dataset. This provides a generalizable, data-driven solution for few-shot, variable-condition fault diagnosis in realistic industrial scenarios.

Keywords
rolling bearing fault diagnosis, generative adversarial network, data imbalance, variable operating conditions, composite label vector

1. Introduction

Rolling bearings are critical components in rotating machinery, widely deployed in aerospace, manufacturing, energy, and transportation sectors. Statistical studies indicate that bearing-related failures account for approximately 40% – 50% of all rotating machinery breakdowns, frequently leading to costly unplanned downtime, significant economic losses, and even catastrophic safety incidents [1]. For instance, a single unplanned shutdown of a wind turbine gearbox can cost tens of thousands of dollars, while bearing failures in high-speed rail or aviation systems can pose direct threats to human safety. Consequently, data-driven intelligent fault diagnosis has become a cornerstone of modern predictive maintenance strategies. However, the development of robust and generalizable diagnostic models faces two persistent and severe challenges in real-world industrial scenarios: (i) data imbalance, where fault samples are inherently scarce compared to abundant normal operational data, as equipment typically operates in a healthy state for the vast majority of its service life; and (ii) variable operating conditions, where loads, speeds, and environmental factors fluctuate continuously during actual

(*) Corresponding author.
E-mail addresses: L. Wei (ORCID: 0000-0003-2416-6630) weilunpan@hrbeu.edu.cn, Q. Wu (ORCID: 0000-0002-5327-7068) wuqilong@hrbeu.edu.cn, Y. Song (ORCID: 0000-0002-4313-8312) songyj_2017@163.com, H. Wang (ORCID: 0009-0006-0293-2153) wang_he@hrbeu.edu.cn

operation, causing significant shifts in the vibration signal characteristics. The co-existence of these two challenges severely restricts the generalization ability of conventional diagnostic models. Traditional signal processing methods and standard deep learning classifiers often struggle to maintain performance when deployed across different operating regimes, particularly when labeled fault data under specific conditions is extremely limited or entirely unavailable [2].

To address the data scarcity issue, virtual fault signal generation based on deep generative models has emerged as a promising frontier. Among these, Generative Adversarial Network (GAN) has become the state-of-the-art technique for synthesizing realistic fault samples to augment training datasets. Early studies primarily focused on stabilizing training to handle basic imbalance. For instance, multi-scale and residual architectures were introduced to enhance feature extraction capabilities [3,4]. More recently, researchers have focused on generating high-fidelity data under small-sample constraints. Notably, in 2025, Zhang et al. [5] proposed a bidirectional interaction-guided GAN to balance datasets in complex environments, and Li et al. [6] developed a mapping-based GAN framework to estimate fault characteristics. Similarly, stability-focused approaches, such as the gradient penalty optimizations by Qin et al. [7] and Liu et al. [8], have significantly improved the convergence of virtual signal generation. Furthermore, recent works have explored multi-domain feature transformation [9], time-efficient GAN architectures [10], and advanced heterogeneous graph learning frameworks for multi-modal and multi-condition diagnosis [11] to handle the growing complexity of industrial fault scenarios, underscoring the active development and remaining challenges in this field.

Despite these advancements, a systematic review of the state of the art reveals two fundamental and interrelated gaps that have not been adequately addressed, forming the core motivation of this work. The first gap lies in the lack of physical controllability in label design. Most existing GAN-based methods [12–14] and even recent Transformer-based variants [15,16] rely on discrete, one-hot encoded labels to represent fault types and operating conditions (e.g., classifying "1 HP" and "2 HP" loads as independent Class A and Class B). This discrete representation fails to encode the continuous physical nature of operating parameters. Consequently, existing models cannot learn the underlying physical mapping between operating conditions (e.g., load) and signal features, restricting them to generating data only for seen conditions. They lack the capability to "interpolate" or synthesize virtual signals for unseen or intermediate operating conditions, which is crucial for variable-condition diagnosis [17,18]. Second, current methods often suffer from inadequate condition injection and training instability. When dealing with multi-domain generation [19,20], standard conditional GANs often employ simple concatenation to inject label information. This shallow interaction is insufficient to guide the generator in distinguishing subtle spectral differences caused by varying loads or fault sizes. Furthermore, the imbalance in learning speeds between the generator and discriminator often leads to mode collapse, a problem highlighted in recent reviews of industrial data generation [21,22]. Recent studies have further attempted to address these challenges from different perspectives: Yang et al. [23] proposed a Variational Stacked Contractive-Auxiliary Classifier GAN (VSC-ACGAN) model to improve generation quality for imbalanced bearing fault samples, while Zhao et al. [24] developed a MultiConditional Variational AutoEncoder GAN (MCVAE-GAN) to tackle signal scarcity and sample diversity in harmonic reducer fault diagnosis. However, these methods still rely on discrete class labels and lack explicit encoding of continuous physical operating parameters, leaving the challenge of physically meaningful and controllable generation across heterogeneous operating regimes largely unresolved.

To address these limitations, this paper proposes an IGAN framework driven by a 5-dimensional CLV. Unlike traditional approaches that treat operating conditions as discrete categories, our method explicitly encodes physical information (Load, Fault Diameter) alongside fault location, enabling the model to learn a continuous physical manifold. This allows for precise control over the generated signals and the ability to synthesize high-fidelity data even for unseen operating conditions. The core innovations and contributions of this study are summarized as follows:

1. Unlike conventional one-hot labeling [12,15] which isolates operating conditions, we design a novel 5D CLV that encodes continuous physical parameters (load and

fault size) to ensure physical consistency. This innovation enables the generator to capture the continuous evolution of fault features, facilitating label vector interpolation to synthesize high-fidelity fault signals for entirely unseen operating conditions (e.g., generating 1 HP data when trained only on 0, 2, and 3 HP).

2. To overcome the limitations of simple concatenation [14], we implement a robust condition injection mechanism using a high-dimensional mapping strategy. The label vectors are projected into a higher-dimensional feature space before fusion. This ensures that the physical condition information exerts a strong, precise guidance on the generation process, enhancing the spectral fidelity of the virtual signals.
3. Addressing the training instability observed in recent GAN variants [7,8], we employ an ALR strategy. This prevents the discriminator from overpowering the generator early in training, ensuring stable convergence and high-quality data generation.
4. The remainder of this paper is organized as follows: Section 2 reviews related work; Section 3 details the proposed method; Section 4 presents the experimental design and results analysis; and Section 5 concludes the paper.

2. Related work

2.1. Generative adversarial networks

The GAN is an advanced type of deep generative model. Structurally (as shown in Figure 1), the framework consists of two competing neural networks: the Generator (G) and the Discriminator (D) [25].

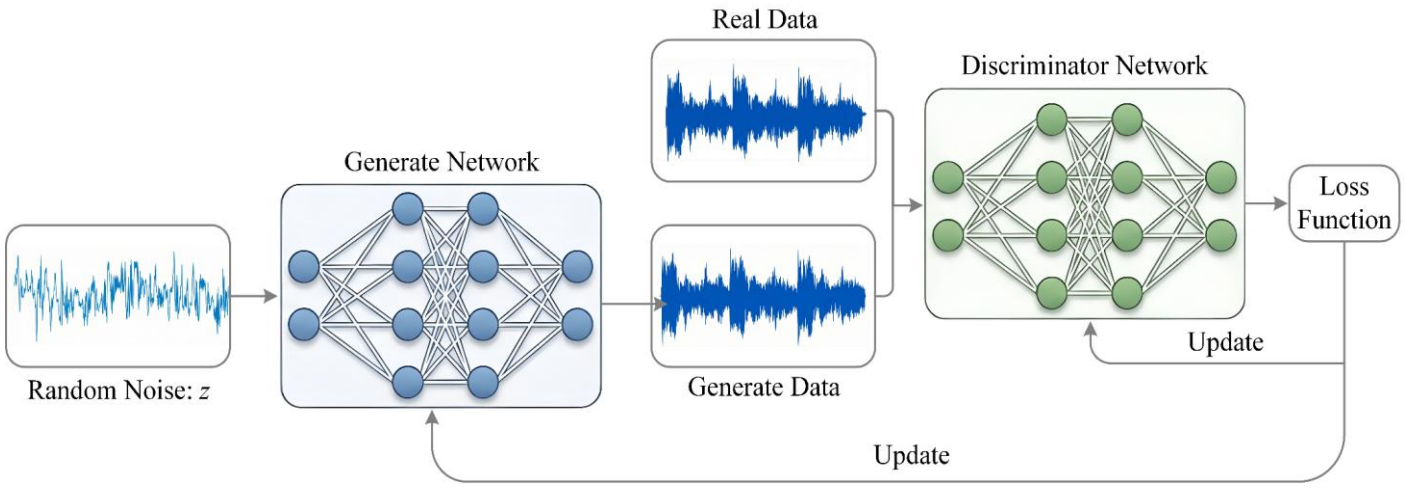

Figure 1. Original GAN Architecture.

The core mechanism of GAN is a dynamic adversarial process, aiming to optimize the model through a "zero-sum game" between the Generator (G) and the Discriminator (D). Specifically, the Generator (G)'s objective is to learn the latent distribution of the real data, thereby generating synthetic data that is sufficiently "realistic," while the Discriminator (D)'s objective is to act as a binary classifier, accurately distinguishing whether an input sample comes from the real data distribution or the synthetic data distribution generated by G. During the training process, G is continually optimized to minimize D's discrimination accuracy (i.e., to "fool" D), while D is optimized to maximize its discrimination accuracy. This adversarial mechanism forces the two networks to co-evolve [26]. Ideally, training ultimately reaches a Nash Equilibrium: at this point, the distribution of the pseudo-data generated by G has converged to the real data distribution, and D cannot effectively differentiate between the real and synthetic samples (i.e., the discrimination probability approaches 0.5), indicating that the Generator has acquired the ability to generate high-fidelity data.

2.2. Design of the label vector

To enable a GAN to generate data for specified physical states under variable operating conditions, it must be provided with precise conditional label information. Although traditional fault diagnosis methods (such as envelope analysis based on bearing characteristic frequencies) are well-established, this paper aims to construct a label vector that simultaneously reflects the

operating condition, fault severity, and fault category [27]. In view of this, this paper proposes a Composite Label Descriptor (CLD) method for IGAN training. This method utilizes a 5-dimensional vector (as shown in Figure 2), which explicitly encodes the following three critical physical attributes: Operating Condition Information (1st dimension), which uses the numerical value of horsepower (HP) representing the equipment load; Fault Size (2nd dimension), which uses the numerical value of the fault diameter (unit: mm) to characterize the fault severity; and Fault Location (3rd–5th dimensions), which uses one-hot encoding representation corresponding to the three health states: "No Fault" (f_i), "Inner Race Fault" (f_bpfi), and "Outer Race Fault" (f_bpfo). This label design scheme (illustrated in Figure 3 example) parameterizes the equipment's running state and health status, allowing the Generator (G) to learn and reproduce the data characteristics under different physical conditions.

Load	Fault diameter	f_i	f_bpfi	f_bpfo

Figure 2. Proposed label description method.

0	0	1	0	0

(a) no load, no fault

1	0.1778	0	1	0

(b) 1 HP Load, 0.007 inch fault diameter, inner race fault

2	0.3556	0	1	0

(c) 2 HP Load, 0.014 inch fault diameter, inner race fault

3	0.5334	0	0	1

(d) 3 HP Load, 0.021 inch fault diameter, outer race fault

Figure 3. Examples of labels under different operating conditions and faults.

3. Proposed method

3.1. Overall framework of the proposed IGAN

This paper proposes an IGAN framework, whose structure is shown in Figure 4. In this framework, the operation of the Generator (G) and the Discriminator (D) is constrained by the label information y as a condition. Specifically, the task of the Generator G is to learn the data distribution of $P(x \mid y)$. It receives a random noise z sampled from a prior distribution (such as Gaussian distribution) and a conditional label y as input, i.e., $G(z, y)$, aiming to synthesize a pseudo-data sample x_{fake} that is consistent with the physical state described by the label y. The task of the Discriminator D is to act as a conditional discriminator. It receives a (sample, label) data pair (x, y) as input, where the data sample x can either come from the real dataset x_{real} or from the Generator x_{fake}. The objective of D is to accurately evaluate the authenticity of the sample x under the given condition y. Through the adversarial game between G and D, the model is ultimately driven to generate high-fidelity conditional data.

3.2. Generator (G)

The network architecture of the Generator G is shown in Figure 5. It is designed as a conditional network based on a Multi-Layer Perceptron [28]. Its core task is to map a prior noise vector z and a conditional label y to a high-dimensional pseudo-data sample x_{fake}. The network adopts a structure of dual independent inputs followed by upsampling:

1. Input Layers: The network receives two separate inputs: Noise Branch: A 100-dimensional prior noise vector z is mapped to a 160-dimensional feature through the fully connected layer Fc_{1-1}. Condition Branch: A 5-dimensional conditional label y is mapped to a 96-dimensional feature through the fully connected layer Fc_{1-2}.
2. Feature Fusion and Upsampling: The features from the above two branches are concatenated into a 256-dimensional fused vector. This vector then undergoes a series of fully connected layers (Fc_2 and Fc_3) for stepwise upsampling, with the dimension transformation being $256 \rightarrow 512 \rightarrow 1024$.
3. Output Layer: Finally, the 1024-dimensional feature vector is mapped to a 512-dimensional pseudo-data sample through the output layer Fc_4.
4. Activation Functions: All hidden layers ($Fc_{1-1}, Fc_{1-2}, Fc_2, Fc_3$) use LeakyReLU as the activation function. The output layer Fc_4 uses the Sigmoid function to ensure the generated samples are normalized.

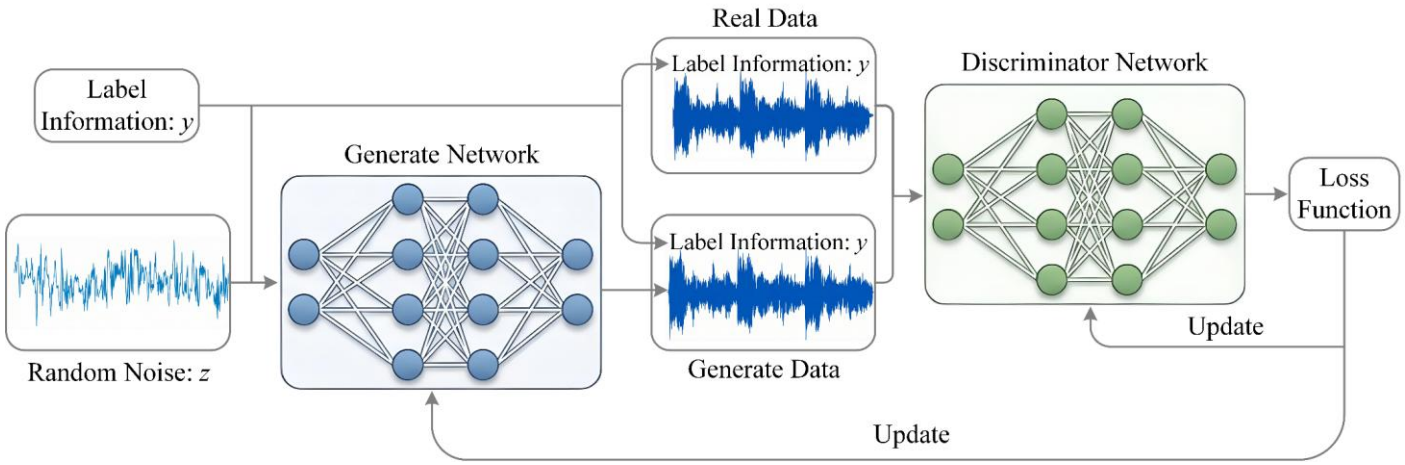

Figure 4. Overall architecture of the proposed IGAN.

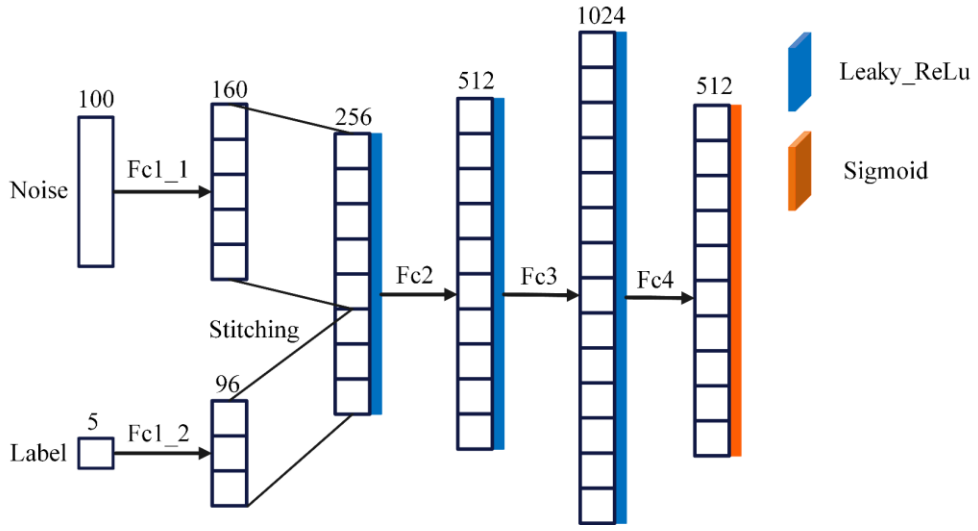

Figure 5. Detailed network architecture of the generator in the proposed IGAN.

Table 1. Generator hyperparameters.

Parameter	Value
Batch Size	128
Learning Rate	0.00125
Training Batches	Experiment I: 850; Experiment II: 1100
StepLR Scheduler	Batches: 300, Decay Rate: 0.081
Adam Optimizer	Betas1: 0.5, Betas2: 0.999
Generator Parameter Initialization	Normal Distribution Mean=0, Std=0.002

3.3. Discriminator (D)

The network architecture of the Discriminator D is shown in Figure 6. It is designed as a conditional discriminator based on a Multi-Layer Perceptron [29]. The core task of D is to assess the consistency between the input data x (either real sample x_{real} or pseudo-sample x_{fake}) and the conditional label y, and output a scalar value to judge its authenticity.

The network adopts a structure of dual independent inputs followed by downsampling:

1. Input Layers: D uses a dual-branch input structure. Data Branch: The 512-dimensional sample x passes through the fully connected layer Fc_{1-1} and is mapped to a 640-dimensional feature. Condition Branch: The 5 -dimensional label vector y passes through the fully connected layer Fc_{1-2} and is mapped to a 384-dimensional feature.
2. Feature Fusion: The feature vectors from the two branches are concatenated into a 1024dimensional fused

vector.

3. Feature Extraction and Downsampling: This 1024-dimensional vector then undergoes a series of fully connected layers (Fc_2 to Fc_4) for stepwise downsampling, with the dimension transformation being $1024 \rightarrow 512 \rightarrow 256 \rightarrow 128$.
4. Output Layer: Finally, the 128 -dimensional feature vector is mapped to a single neuron output via Fc_5.
5. Activation Functions: All hidden layers (Fc_{1-1} to Fc_4) use the LeakyReLU activation function. The output layer Fc_5 uses the Sigmoid function, and its output value (range $[0,1]$) represents the probability that the input sample x is judged as "real" under the given condition y.

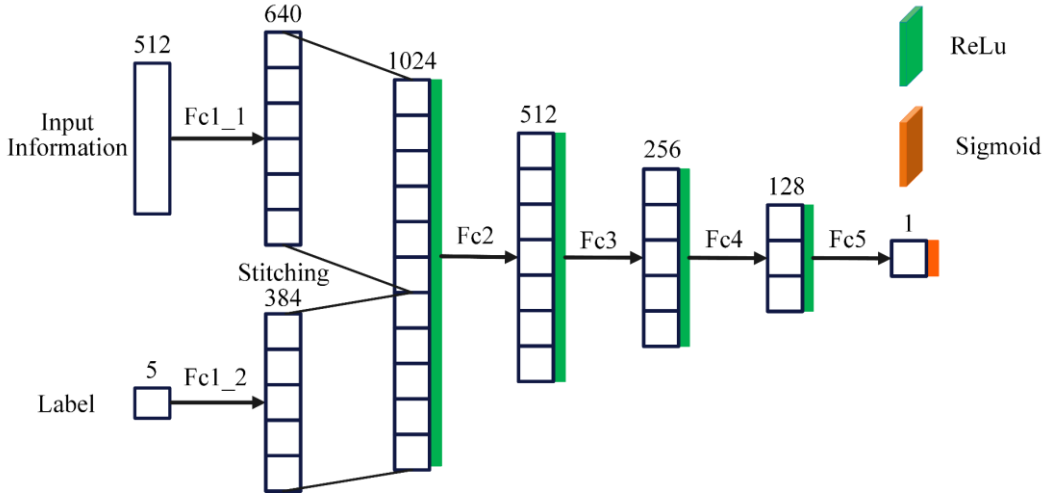

Figure 6. Detailed network architecture of the discriminator in the proposed IGAN.

Table 2. Discriminator hyperparameters.

Parameter	Value
Batch Size	128
Learning Rate	0.0001
Training Batches	Experiment I: 850; Experiment II: 1100
StepLR Scheduler	Batches: 300, Decay Rate: 0.092
LeakyReLU	0.0015
Adam Optimizer	Betas1: 0.5, Betas2: 0.999
Generator Parameter Initialization	Normal Distribution Mean=0, Std=0.002

3.4. Network design principles and training strategies

To achieve efficient data generation, this paper performs targeted optimization on the network design and training strategies, the core principles of which are summarized as follows:

1. Information Injection Strategy: To ensure that the Generator G and Discriminator D fully utilize the information from the conditional label y (5-dimensional), this paper does not adopt simple concatenation. As shown in Figure 5 and Figure 6, the label vector is mapped to a high-dimensional feature representation by passing through independent fully connected layers (Fc_{1-2}) in G and D respectively (G: $5 \rightarrow 96$ dimensions; D: $5 \rightarrow 384$ dimensions). This approach provides the network with a higher-dimensional label representation, which can more effectively guide the data generation and discrimination processes after concatenation.
2. Asymmetric Learning Rates: To address the problem of the Discriminator D becoming overly powerful too quickly, leading to gradient vanishing in GAN training, this paper employs an ALR strategy (refer to Table 1 and Table 2). G uses a relatively higher initial learning rate (0.00125) to promote its rapid exploration of the data distribution, while D uses a lower learning rate (0.0001) to prevent it from prematurely overwhelming G. Additionally, G 's learning rate decay (0.081) is faster than D 's (0.092), which helps the model converge smoothly to equilibrium in the later stages of training.

3. Training Iterations and Hardware Configuration: As shown in Table 1 and Table 2, Experiment I and Experiment II use different total training batches (850 and 1100, respectively). This is to accommodate the difference in the scale of the training datasets between the two experiments, ensuring that the model can achieve convergence across different data volumes. All experiments are conducted on an NVIDIA RTX 3070 Ti GPU (8GB), with a uniform Batch Size of 128 to strike a balance between training efficiency and memory usage.

4. Experimental design and results analysis

4.1. Experimental bench and dataset description

This study employs the internationally recognized Case Western Reserve University (CWRU) Bearing Dataset as the experimental data source [30]. To facilitate a clear understanding of the data acquisition process, the structure of the experimental test rig is illustrated in Figure 7.

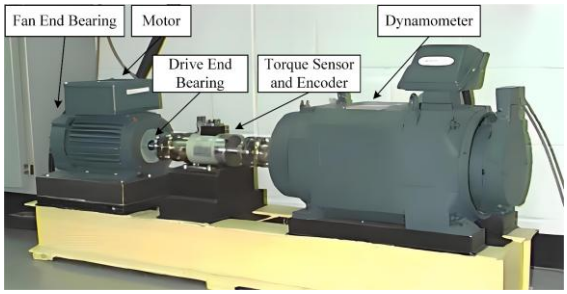

Figure 7. CWRU experimental test rig.

As shown in Figure 7, the test rig consists of a 2 hp (1.5 kW) three-phase induction motor, a torque transducer/encoder, and a dynamometer utilized to apply different loads. The motor shaft is supported by 6205-2RS JEM SKF deep groove ball bearings. Vibration signals were collected using accelerometers attached to the motor housing with magnetic bases at the drive end (DE) of the motor, with a sampling frequency of 12 kHz.

To simulate realistic bearing damage, single-point defects were introduced to the test bearings using Electrical Discharge Machining (EDM). While the CWRU database contains various fault types and locations, to validate the effectiveness of the proposed method under variable operating conditions and data imbalance scenarios, this experiment selects a specific data subset. This subset covers four operating conditions (loads 0, 1, 2, 3 HP) and three health states (Normal, Inner Race Fault, Outer Race Fault). All fault samples in this subset use a single fault diameter of 0.007 inches (0.1778 mm). Table 3 details the length of the selected raw data and the corresponding label encoding. It is clear from the data lengths that the dataset used in this study exhibits a significant class-imbalance characteristic, where the number of samples for the Normal state far exceeds that of any single fault category. This characteristic simulates the typical scenario of fault sample scarcity in industrial practice and constitutes the core motivation for adopting the GAN for data augmentation in this paper.

Table 3. Raw dataset description and label encoding.

Operating Condition	Fault Diameter	Fault Location	Data Length	Label
No Load	0.007	Normal	243938	[0, 0, 1, 0, 0]
		Inner Race	121265	[0, 0.1778, 0, 1, 0]
		Outer Race	121991	[0, 0.1778, 0, 0, 1]
1 HP Load	0.007	Normal	243903	[1, 0, 1, 0, 0]
		Inner Race	121991	[1, 0.1778, 0, 1, 0]
		Outer Race	122426	[1, 0.1778, 0, 0, 1]
2 HP Load	0.007	Normal	243903	[2, 0, 1, 0, 0]
		Inner Race	122136	[2, 0.1778, 0, 1, 0]
		Outer Race	121410	[2, 0.1778, 0, 0, 1]
3 HP Load	0.007	Normal	245643	[3, 0, 1, 0, 0]
		Inner Race	122917	[3, 0.1778, 0, 1, 0]
		Outer Race	122571	[3, 0.1778, 0, 0, 1]

4.2. Data Preprocessing

To make the raw time-series signals suitable for the GAN model, the preprocessing procedure involves two steps: time-domain sampling and frequency-domain transformation:

1. Time-Domain Sampling: First, the one-dimensional raw vibration signals in Table 3 are sampled. This paper uses a non-overlapping sliding window with a length of 1024 data points to slice the signal [31]. This window length is sufficient to capture information for one complete fault cycle, and the non-overlapping design ensures the statistical independence between samples. Remaining

data shorter than one window length is discarded. After sampling, the sample counts for each category are statistically summarized in Table 4.

2. Frequency-Domain Transformation: The motivation for using frequency- domain features is that different fault types (e.g., inner race/outer race) exhibit distinct energy distributions in the frequency domain. Therefore, we apply Fast Fourier Transform (FFT) to each 1024-point time-domain sample to extract its frequency-domain characteristics [32]. Since the input signal is a real number, we truncate its single-sided spectrum (corresponding to the 0-6000 Hz frequency band), resulting in a 512-dimensional feature vector. This 512-dimensional vector will serve as the final input data for the subsequent GAN model and classifier.

Table 4. Sample counts in the preprocessed dataset.

Operating Condition	Fault Diameter	Fault Location	Raw Data Sample Count
No Load	0.007	Normal	238
		Inner Race	118
		Outer Race	119
1 HP Load	0.007	Normal	238
		Inner Race	119
		Outer Race	119
2 HP Load	0.007	Normal	238
		Inner Race	119
		Outer Race	118
3 HP Load	0.007	Normal	239
		Inner Race	120
		Outer Race	119

4.3. Experiment I

4.3.1. Experimental setup and objective

The core objective of Experiment I is to validate the effectiveness of the proposed IGAN model and label strategy in generating high-fidelity data under variable operating conditions, and to assess the application value of this generated data in solving the class-imbalance problem. This experiment simulates a typical industrial scenario where "health data is sufficient, but fault data is scarce." We extract samples only from the eight minority classes (i.e., inner race/outer race faults under four loads) of the preprocessed dataset (Table 4) to form the training set for the proposed IGAN. The detailed composition of this training set is shown in Table 5. The evaluation for this experiment includes: (a) Model Convergence Analysis, (b) Frequency Domain Assessment of Generated Data Quality, (c) Quantitative Analysis of Generated Data Fidelity (via correlation), and (d) Downstream Task Evaluation (covering both Classification Accuracy and Noise Robustness).

Table 5. Experiment I: training set composition and label encoding.

Operating Condition	Fault Diameter (mm)	Fault Location	Label	Index
No Load	0.007	Inner Race	[0, 0.1778, 0, 1, 0]	1
		Outer Race	[0, 0.1778, 0, 0, 1]	5
1 HP Load	0.007	Inner Race	[1, 0.1778, 0, 1, 0]	2
		Outer Race	[1, 0.1778, 0, 0, 1]	6
2 HP Load	0.007	Inner Race	[2, 0.1778, 0, 1, 0]	3
		Outer Race	[2, 0.1778, 0, 0, 1]	7
3 HP Load	0.007	Inner Race	[3, 0.1778, 0, 1, 0]	4
		Outer Race	[3, 0.1778, 0, 0, 1]	8

4.3.2. Model convergence analysis

Figure 8 shows the curves of the Generator Loss ($\mathcal{L}_G$) and Discriminator Loss ($\mathcal{L}_D$) over 850 training batches in Experiment I. The curve clearly reflects the dynamic adversarial game between the two networks. Initial Phase (approx. 0-200 batches): $\mathcal{L}_D$ drops rapidly, indicating that the Discriminator D can easily distinguish the low-quality pseudo-samples generated by G, with D dominating the game at this stage. Adversarial Phase (approx. 200-400 batches): As G begins to

capture the real data features, $\mathcal{L}_G$ gradually decreases; the difficulty of discrimination for D increases, leading to a significant rebound in $\mathcal{L}_D$. Equilibrium Phase (approx. 400-850 batches): Both $\mathcal{L}_G$ and $\mathcal{L}_D$ converge to a low, stable level and oscillate slightly around an Equilibrium point. This indicates that G and D have reached a Nash Equilibrium state, and the model has converged.

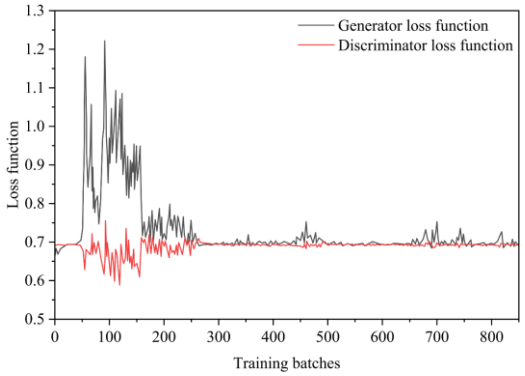

Figure 8. Experiment I: loss function curves during model training.

4.3.3. Frequency domain assessment of generated data quality

To qualitatively assess the quality of the generated data, Figure 9 compares the frequency domain spectra of real data and the pseudo-data generated by the proposed IGAN under all 8 conditions. As shown, the generated samples exhibit high fidelity across all conditions, accurately reproducing the spectral structure of the real data, including the positions and amplitude relationships of the main harmonic peaks. Concurrently, the minor differences observed in local regions (such as peak amplitudes and baseline noise) suggest that the model did not simply overfit the training samples but successfully learned the underlying data distribution, generating new samples with diversity.

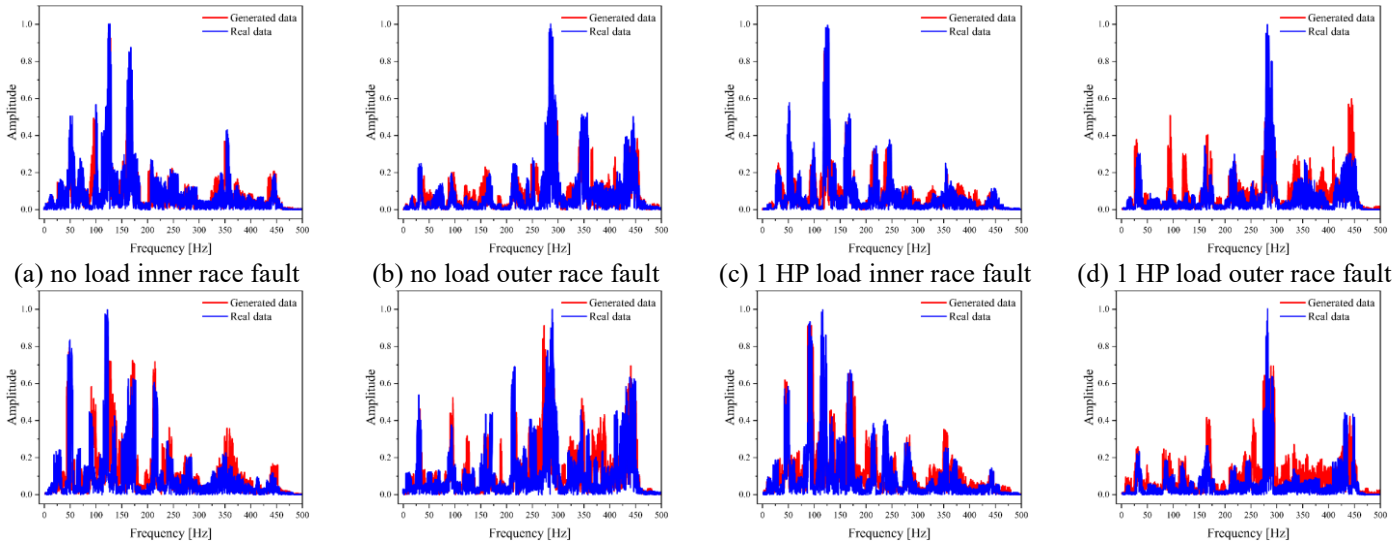

(a) no load inner race fault (b) no load outer race fault (c) 1 HP load inner race fault (d) 1 HP load outer race fault

(e) 2 HP load inner race fault (f) 2 HP load outer race fault (g) 3 HP load inner race fault (h) 3 HP load outer race fault

Figure 9. Experiment I: frequency domain comparison of generated samples and real samples.

4.3.4. Quantitative analysis of generated data fidelity

For further quantitative evaluation, we computed the Pearson correlation coefficient matrix for 16 types of data (8 classes of real data, indexed 1-8; and 8 classes of corresponding generated data, indexed 9-16), as shown in Figure 10. The matrix reveals the physical properties of the real data: The correlation between Inner Race Faults (1-4) is relatively low, indicating that their features are highly sensitive to changes in operating conditions (load). Conversely, the correlation between Outer Race Faults (5-8) is relatively high, suggesting their features are more stable across different operating conditions. Generated Data Fidelity (Diagonal Blocks): The key diagonal blocks of the matrix (i.e., Real Inner Race 1-4 vs. Generated Inner Race 9-12; Real Outer Race 5-8 vs. Generated Outer Race 13-16) all show extremely strong positive correlation. This quantitatively confirms the high fidelity of the proposed IGAN, indicating that the Generator successfully learned and reproduced the precise features for each specific operating condition and fault location. Generated Data Specificity (Off-Diagonal Blocks): The low correlation in the off-diagonal blocks confirms that the Generator has not undergone mode collapse and is capable of

generating data with high specificity based on the conditional label y.

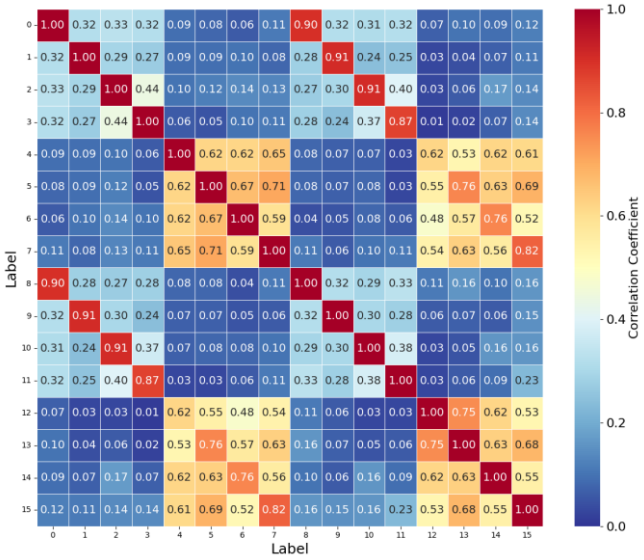

Figure 10. Experiment I: correlation matrix of real samples and generated samples.

4.3.5. Downstream task evaluation: classification accuracy

To validate the practical application value of the generated data, we use the generated pseudo-samples to perform data augmentation on the original imbalanced dataset (Table 4). In the experiment, we incrementally add 30 pseudo-samples at a time for four iterations (totaling 120 pseudo-samples) to the 8 minority classes in the original training set. Evaluation is performed using four baseline classifiers (KNN, SVM, MLP, and 1D-CNN) with an 8:2 train-test split, averaging the results over 10 repeated experiments.

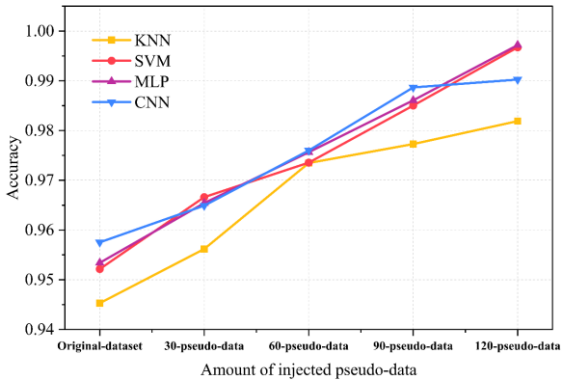

Figure 11. Experiment I: impact of data augmentation on classifier accuracy.

As shown in Figure 11, the diagnostic accuracy of all four classifiers shows a significant and monotonic increase as the generated pseudo-samples are used to augment the training set. This proves the effectiveness of the pseudo-data generated in this paper, as they provide the classifiers with more diverse information, helping them learn more robust decision boundaries on class-imbalanced data.

4.3.6. Downstream task evaluation: noise robustness

To simulate a realistic industrial environment, we further evaluate the impact of data augmentation on the model's noise robustness. Gaussian white noise with varying intensities, corresponding to a Signal-to-Noise Ratio (SNR) ranging from 30 dB (low noise) to 0 dB (strong noise), is injected into both the training and test sets after the 8:2 split.

As shown in Figure 12, deep models (MLP, CNN) exhibit stronger intrinsic robustness at low SNRs compared to traditional models (SVM, KNN). At almost all SNR levels, the classifiers trained with data augmentation consistently outperform the baseline models trained using only the original data. This performance improvement is particularly pronounced on MLP and CNN. This suggests that by training on a more diverse and balanced dataset, the classifiers extract more generalizable features, thereby significantly enhancing their robustness in strong noise environments.

4.3.7. Comparative analysis with alternative generative models

To further demonstrate the superiority of the proposed IGAN, we compared it with four widely used generative models in fault diagnosis: the standard Conditional GAN (cGAN) [33], the VSC-ACGAN [23], the MultiConditional Variational AutoEncoder GAN (MCVAE-GAN) [24], and the WGAN-GP [34]. All models were trained on the same imbalanced training set (Experiment I configuration) and used to generate pseudo-samples to augment the minority classes. For fair comparison, each generative model was used to generate 120 pseudo-samples per minority class to augment the training set.

We employed two metrics for evaluation:

1. Maximum Mean Discrepancy (MMD) [35]: A lower MMD value indicates that the distribution of generated data is closer to the real data distribution.
2. Classification Accuracy (with CNN): The accuracy of the CNN classifier trained on the augmented dataset (Real + Generated), which reflects the practical utility of the generated data.

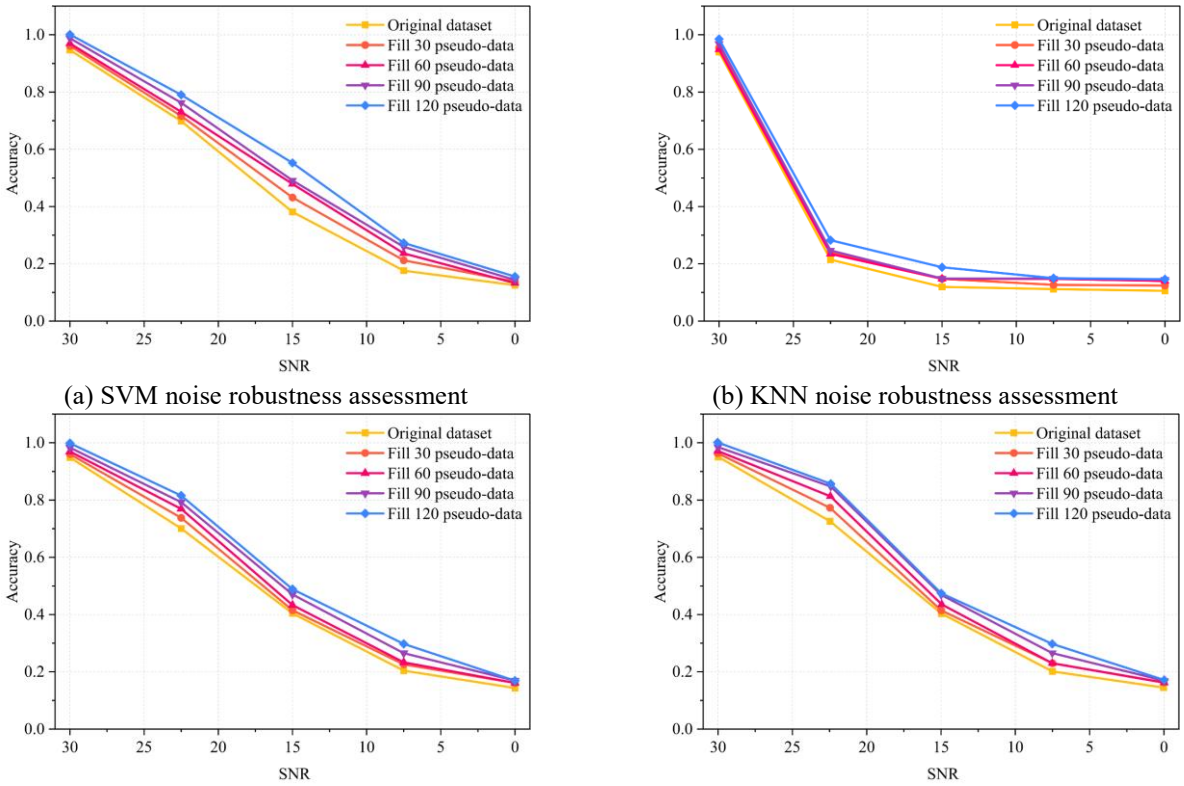

(a) SVM noise robustness assessment

(b) KNN noise robustness assessment

(c) MLP noise robustness assessment

(d) CNN noise robustness assessment

Figure 12. Experiment I: impact of data augmentation on model noise robustness.

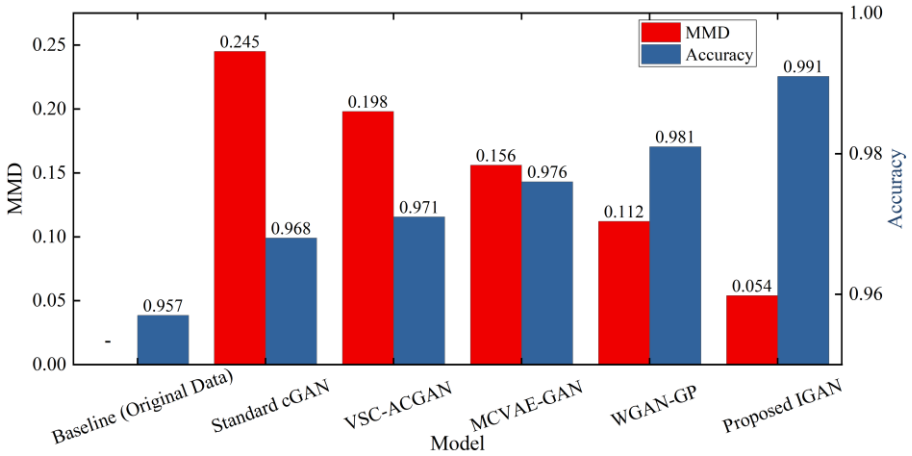

Figure 13. Comparison with baseline generative models.

Figure 13 presents the comparative results. The standard cGAN yielded the highest MMD (0.245) and the lowest accuracy improvement, primarily due to the occurrence of mode collapse during training. VSC-ACGAN improved the classification accuracy to 97.1% (MMD: 0.198) by leveraging its auxiliary classifier to encourage class-specific generation; however, its one-hot label representation still limits its ability to capture the continuous physical relationship between operating conditions. MCVAE-GAN, which combines variational inference with adversarial training, achieved a better MMD of 0.156 and an accuracy of 97.6%, demonstrating more stable latent space learning. WGAN-GP further improved stability and signal quality (MMD: 0.112, Accuracy: 98.1%) through its gradient penalty mechanism. However, our proposed IGAN achieved the best performance across both metrics (MMD: 0.054, Accuracy: 99.1%). This superiority is attributed to the synergistic effect of three key factors: the 5D CLV provides precise physical constraints, the high-dimensional injection mechanism ensures effective condition guidance, and the ALR strategy balances the training dynamics.

4.3.8. Ablation study: impact of CLV

To systematically isolate the specific contribution of each proposed innovation, we conducted a comprehensive ablation

study with four model variants, as detailed in Table 6.

1. IGAN-Base: Uses standard one-hot discrete labels with simple concatenation (no high-dimensional FC mapping for labels) and symmetric learning rates (same LR for G and D). This serves as the most basic conditional GAN configuration using our network architecture.
2. IGAN-Inject: Adds the high-dimensional injection mechanism (FC mapping for labels) to IGAN-Base, while retaining one-hot labels and symmetric learning rates. This isolates the contribution of the injection strategy.
3. IGAN-Discrete: Adds the ALR strategy to IGAN-Inject, while retaining one-hot labels. This is equivalent to the proposed architecture without the 5D CLV.
4. Proposed IGAN: Uses the full configuration with the 5D CLV, high-dimensional injection, and ALR strategy.

Table 6. Comprehensive ablation study.

Model	Label Type	Injection	ALR	MMD	CNN Accuracy
IGAN-Base	One-hot	Concatenation	No	0.152	96.5%
IGAN-Inject	One-hot	FC Mapping	No	0.112	97.3%
IGAN-Discrete	One-hot	FC Mapping	Yes	0.082	97.9%
Proposed IGAN	5D Composite	FC Mapping	Yes	0.054	99.1%

The results in Table 6 reveal the incremental contribution of each component:

(1) Effect of the Injection Mechanism: Comparing IGAN-Base (Concatenation) with IGAN-Inject (FC Mapping), the MMD decreased from 0.152 to 0.112, and accuracy improved from 96.5% to 97.3%. This confirms that projecting the label vector into a higher-dimensional feature space before fusion provides a richer conditional representation, enabling the generator and discriminator to more effectively utilize the condition information.

(2) Effect of the ALR Strategy: Comparing IGAN-Inject (Symmetric LR) with IGAN-Discrete (ALR), the MMD further decreased from 0.112 to 0.082, and accuracy improved from 97.3% to 97.9%. This demonstrates that the ALR strategy effectively prevents discriminator dominance, leading to more stable training and higher-quality generation.

(3) Effect of the 5D CLV: Comparing IGAN-Discrete (One-hot) with the Proposed IGAN (5D CLV), the MMD decreased from 0.082 to 0.054, and accuracy improved from 97.9% to 99.1%. This most significant improvement proves that the composite labels do not merely act as class identifiers; they impose continuous physical constraints (specifically Load and Defect Diameter) on the generator. This guides the network to learn a smoother and more physically consistent manifold, resulting in generated samples that are more representative of the real fault characteristics.

4.4. Experiment II

4.4.1. Experimental setup and objective

The core objective of Experiment II is to evaluate the generalization ability of the proposed IGAN model proposed in this paper, i.e., its capability to generate high-fidelity data under operating conditions not present in the training data. To this end, we designed a "leave-one-out" mode experiment: all data corresponding to the "1 HP Load" operating condition were deliberately excluded from the original four conditions. As shown in Table 7, the training set for the proposed IGAN only includes fault data under three operating conditions: No Load, 2 HP Load, and 3 HP Load.

Table 7. Experiment II: training set composition (excluding unknown condition).

Operating Condition	Fault Diameter	Fault Location	Label
No Load	0.007	Inner Race	[0, 0.1778, 0, 1, 0]
		Outer Race	[0, 0.1778, 0, 0, 1]
2 HP Load	0.007	Inner Race	[2, 0.1778, 0, 1, 0]
		Outer Race	[2, 0.1778, 0, 0, 1]
3 HP Load	0.007	Inner Race	[3, 0.1778, 0, 1, 0]
		Outer Race	[3, 0.1778, 0, 0, 1]

4.4.2. Model convergence analysis

Figure 14 displays the loss function curves over 1100 training batches in Experiment II. Despite the absence of one operating condition in the training data, the model still demonstrates good convergence. Similar to Experiment I, the model undergoes a fierce adversarial game during the initial phase (approx. 0-200 batches), characterized by a significant peak in $\mathcal{L}_G$ and a corresponding drop in $\mathscr{L}_D$. After approximately 400 batches, both loss functions tend to stabilize, indicating that the model successfully reached Nash Equilibrium even under the condition of "missing" data, and fully converged after 1100 batches.

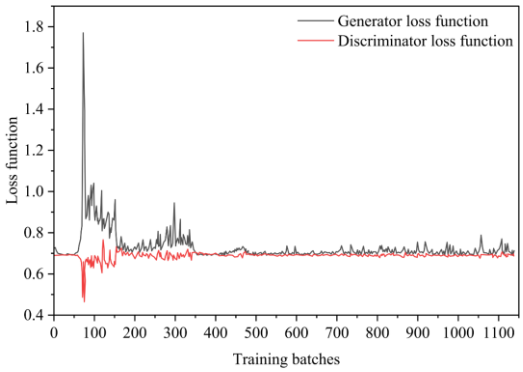

Figure. 14. Experiment II: loss function curves during model training.

4.4.3. Generation quality for known conditions

As a baseline verification of the model, we first generated data for the operating conditions included in the training set (0, 2 3 HP). As shown in Figure 15, the generated pseudo-samples are highly consistent with the corresponding real samples in terms of spectral structure. This confirms that the model's ability to generate known data remains unaffected after excluding the "1 HP Load" data, maintaining both high fidelity and diversity.

4.4.4. Generation quality for unknown conditions

The key to this experiment is to evaluate the model's generation capability for the unknown operating condition (1 HP Load). We provided the trained Generator G with a 100-dimensional random noise z and the conditional labels y corresponding to the "1 HP Load" (i.e., [1, 0.1778, 0, 1, 0] and [1, 0.1778, 0, 0, 1]). As shown in Figure 16, the model successfully generated pseudo-data for this unknown condition. By comparing the frequency domain spectra with the real "1 HP Load" data (which did not participate in training), it is clear that the generated samples highly match the real samples in terms of main spectral peaks and overall distribution. This result strongly proves the effectiveness of the CLV design (Section 2.2) proposed in this paper. The proposed IGAN is not merely memorizing the training data but has successfully learned the latent mapping relationship between the "Load" (1st dimension of the label) and the spectral features. Therefore, the model is able to generalize through interpolation to generate high-fidelity data under entirely new operating conditions that were not included in the training set.

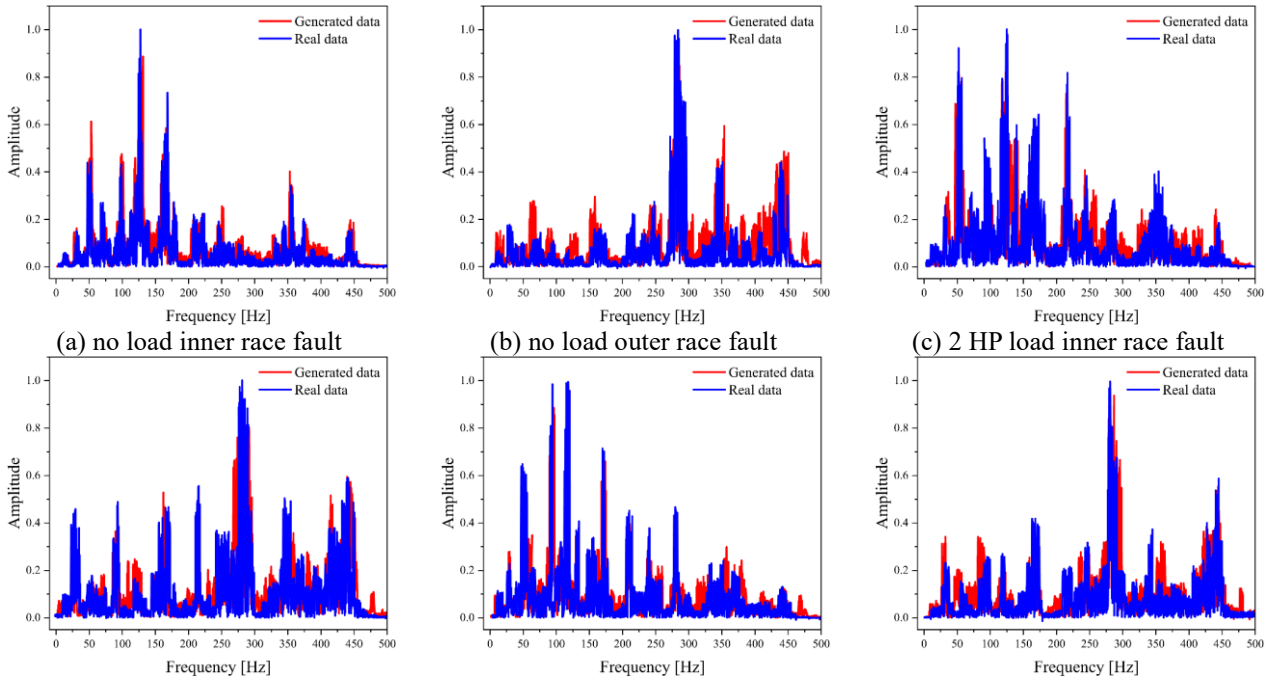

(a) no load inner race fault (b) no load outer race fault (c) 2 HP load inner race fault

(d) 2 HP load outer race fault (e) 3 HP load inner race fault (f) 3 HP load outer race fault

Figure 15. Experiment II: frequency domain comparison for known conditions (within training set).

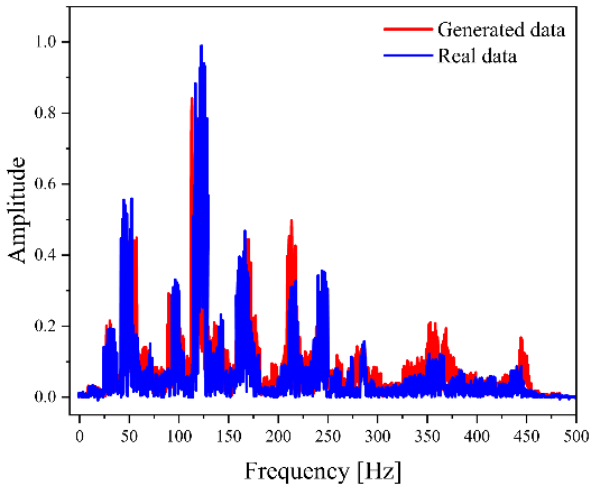

(a) 1 HP load inner race fault

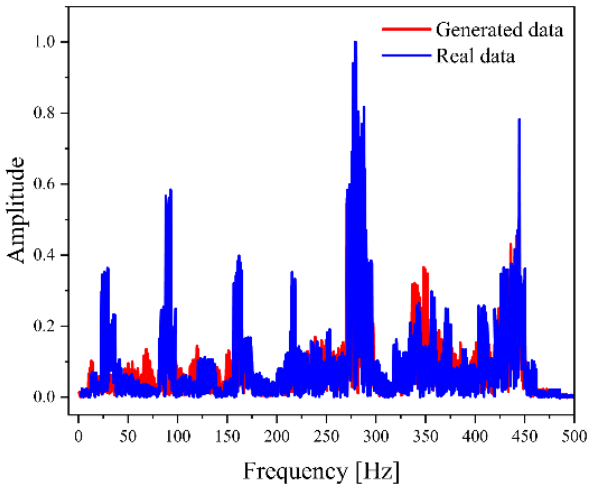

(b) 1 HP load outer race fault

Figure 16. Experiment II: frequency domain comparison for unknown conditions (outside training set).

4.5. Hyperparameter sensitivity analysis

To verify the reproducibility and robustness of the proposed IGAN, we conducted a systematic sensitivity analysis on two critical hyperparameters: the ALR ratio and the dimension of the latent space.

4.5.1. Impact of ALR ratio

The ALR strategy is designed to balance the training speed between the generator and discriminator. We defined the learning rate ratio as $k = lr_d/lr_g$ and evaluated the model's performance under different k values while keeping lr_g fixed. The results are summarized in Table 8.

Table 8. Impact of learning rate ratio (k) on performance.

Ratio ($k = lr_d/lr_g$)	Training Stability	MMD (Lower is better)	CNN Accuracy
1:1 (Standard)	Unstable (Oscillation)	0.145	96.5%
1:4	Moderate	0.089	97.8%
1:12 (Proposed)	Stable (Optimal)	0.054	99.1%
1:20	Slow Convergence	0.076	98.4%

As observed, the standard setting (1:1) led to training instability and higher MMD. The proposed ratio of 1:12 achieved the best equilibrium, allowing the discriminator to provide meaningful gradients without overpowering the generator, resulting in the lowest MMD (0.054) and highest accuracy (99.1%).

4.5.2. Sensitivity to latent space dimension

While the dimension of the 5D CLV is fixed by the physical attributes of the fault signals (Fault Type, Load, and Diameter), the dimension of the random noise vector (z_{dim}) is a structural hyperparameter that affects the generative capacity. We evaluated the model's sensitivity to z_{dim} as shown in Table 9.

Table 9. Sensitivity analysis of latent dimension (z_{dim}).

Latent Dimension (z_{dim})	MMD	CNN Accuracy	Remark
64	0.092	97.5%	Limited capacity
100 (Proposed)	0.054	99.1%	Optimal balance
128	0.058	98.9%	Stable
256	0.065	98.2%	Signs of overfitting

The results indicate that the model performs robustly when z_{dim} is between 100 and 128 . A dimension that is too small (64) limits the diversity of generated samples, while an excessively large dimension (256) introduces unnecessary complexity. The chosen dimension of 100 ensures both high signal quality and classification utility.

4.6. Generalization validation on IMS dataset

To verify the generalization capability of the proposed method

under real-world operating conditions, we extended our validation to the IMS Bearing Dataset generated by the NSF I/UCR Center for Intelligent Maintenance Systems (IMS) [36].

4.6.1. Dataset description and experimental setup

Unlike the CWRU dataset where faults are artificially induced via EDM, the IMS dataset represents a natural run-to-failure process, capturing the gradual degradation of bearings due to fatigue. This aligns closely with realistic industrial maintenance scenarios. The structure of the IMS bearing test rig is illustrated in Figure 17.

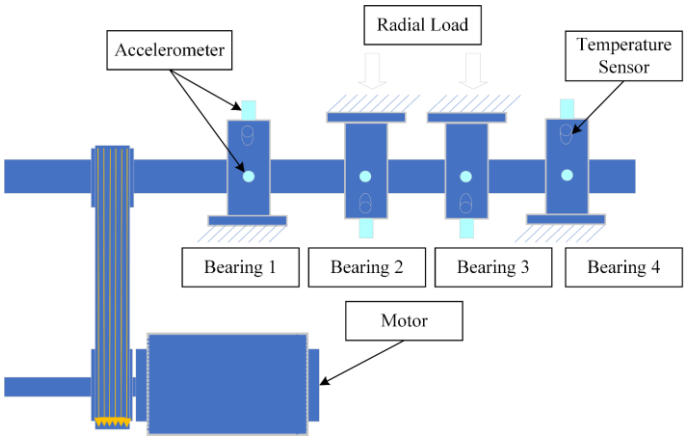

Figure 17. Schematic diagram of the IMS bearing test rig.

4.6.2. Experimental results

We constructed a dataset from the IMS life-cycle data consistent with the label logic defined in Section 2.2. Specifically, the data covers three health states: Normal (f_i), Inner Race Fault (f_bpfi), and Outer Race Fault (f_bpfo). To adapt the proposed 5-dimensional CLV to the natural degradation characteristics of the IMS dataset, we implemented the following mapping strategy:

1. Load (1st Dimension): Since the IMS rig operates under a constant heavy load, the 1st dimension was fixed to the numerical value representing the 6000 lbs radial load, maintaining the physical consistency of the "Operating Condition" input.
2. Fault Diameter (2nd Dimension): Unlike the fixed diameter values in CWRU, IMS faults are naturally evolved cracks. Therefore, the "Fault Diameter" dimension was mapped to a normalized degradation index (derived from the life-cycle timeline) to represent the continuous evolution of fault severity.
3. Fault Location (3rd–5th Dimensions): The one-hot encoded vector was assigned based on the verified failure mode of each bearing. Specifically, the health states were mapped as follows: Normal state (f_i) corresponds to [1, 0, 0], Inner Race Fault (f_bpfi) to [0, 1, 0], and Outer Race Fault (f_bpfo) to [0, 0, 1].
4. We trained the proposed IGAN and the baseline models on this dataset using the same training configuration as Experiment I.

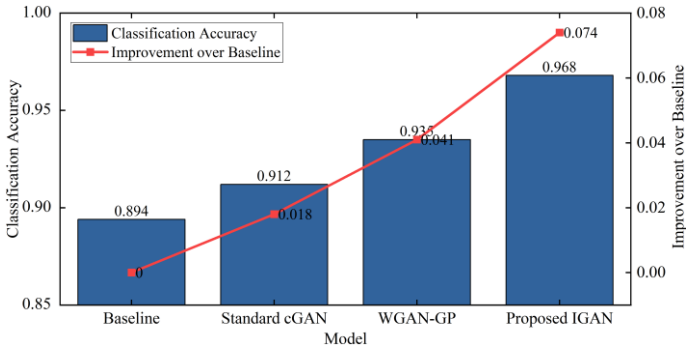

Figure 18. Performance comparison on IMS dataset.

The comparative results are presented in Figure 18. As observed, the classification accuracy on the IMS dataset is generally lower than that on CWRU due to the inherent complexity and strong noise of natural degradation signals; however, the proposed IGAN still demonstrates superior performance, achieving a high accuracy of 96.8%. Notably, Figure 18 highlights the significant improvement over baselines, where the proposed IGAN achieved a substantial boost of +7.4% compared to the raw Baseline (89.4%), proving its ability to generate high-fidelity features that are easily distinguishable by the classifier. Furthermore, the IGAN outperforms other generative models, surpassing the Standard cGAN (91.2%) by 5.6% and WGAN-GP (93.5%) by 3.3%. This indicates that even with natural faults lacking precise "mm-scale" diameter labels, the 5D CLV strategy effectively enables the generator to capture subtle spectral changes and physical constraints associated with degradation, powerfully validating the method's strong generalization ability and potential for deployment in practical industrial scenarios.

4.6.3. Noise robustness validation on IMS dataset

To further verify the practical robustness of the proposed method under conditions that more closely resemble engineering practice, we conducted an additional noise robustness experiment on the IMS dataset. Gaussian white noise

with varying intensities (SNR from 30 dB to 0 dB) was injected into the IMS test data. We compared the CNN classification accuracy of the Baseline (no augmentation) against models augmented by Standard cGAN, WGAN-GP, and the proposed IGAN, respectively. The results are presented in Figure 19.

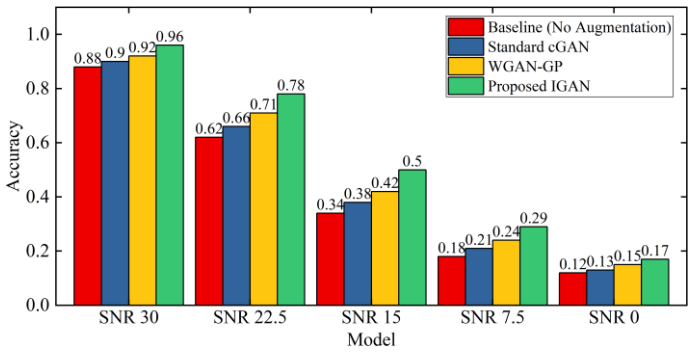

Figure 19. IMS dataset: noise robustness comparison (cnn classifier).

As shown in Figure 19, the overall noise robustness on the IMS dataset is lower than that on the CWRU dataset (Figure 12), which is expected due to the inherent complexity and strong background noise of natural degradation signals. Nevertheless, the proposed IGAN consistently outperforms all baseline methods across all SNR levels. Notably, at moderate noise levels (SNR 15 dB), the IGAN-augmented model achieves an accuracy of 0.50, representing a substantial improvement of +16 percentage points over the non-augmented Baseline (0.34). Even under severe noise conditions (SNR 0 dB), the IGAN maintains a clear advantage. These results confirm that the high-fidelity pseudo-samples generated by the proposed IGAN provide meaningful distributional diversity that enhances the classifier's ability to extract noise-invariant features, validating the method's robustness for practical engineering environments.

5. Conclusion

This paper successfully proposes an IGAN framework driven by a 5-dimensional CLV and ALR to address the challenges of data imbalance and variable operating conditions in rolling element bearing fault diagnosis. Through innovations in label design and conditional injection strategies, the study achieved the synthesis of high-fidelity data under precise physical control of operating condition, fault severity, and location. Experimental validation confirms that the proposed IGAN outperforms state-of-the-art baselines such as cGAN and WGAN-GP in both signal fidelity (lowest MMD) and downstream classification accuracy, while ablation studies verify the critical role of the CLV in learning a continuous physical manifold. Furthermore, the generated data significantly boosts diagnostic accuracy in strong noise environments and successfully synthesizes high-fidelity fault signals for unseen operating conditions via interpolative reasoning. Cross-domain validation on the IMS dataset further proved the model's effectiveness in diagnosing natural degradation faults, confirming its generalization capability beyond artificially induced fault scenarios. Future work will focus on two key directions: (1) collecting and validating the proposed method on actual engineering field data from industrial rotating machinery (e.g., wind turbine gearboxes) to bridge the gap between laboratory benchmarks and real-world deployment; and (2) integrating multi-modal feature inputs, such as combining vibration signals with acoustic emission and temperature data, to enhance the physical richness of the Composite Label Vector.

Acknowledgement

This work was supported by the National Natural Science Foundation of China under Grant No. 72501042.

References

1. Lei L, Li W, Zhang S, Wu C, Yu H. Research Progress on Data-Driven Industrial Fault Diagnosis Methods. Sensors, 2025; 25(9): 2952. doi: 10.3390/s25092952.
2. Fan H, Xue C, Ma J, Cao X, Zhang X. A novel intelligent diagnosis method of rolling bearing and rotor composite faults based on vibration signal-to-image mapping and CNN-SVM. Measurement Science and Technology, 2023; 34(4): 044008. doi: 10.1088/1361-6501/acad90.
3. Liu J, Zhang C, Jiang X. Imbalanced fault diagnosis of rolling bearing using improved MsR-GAN and feature enhancement-driven CapsNet. Mechanical Systems and Signal Processing, 2022; 168: 108664. doi: 10.1016/j.ymssp.2021.108664.
4. Xu K, Kong X, Wang Q, Yang S, Huang N, Wang J. A bearing fault diagnosis method without fault data in new working condition combined dynamic model with deep learning. Advanced Engineering Informatics, 2022; 54: 101795. doi: 10.1016/j.aei.2022.101795.

5. Zhang Z, Yuan X, Ye T, Zhu W, Zhou F. Bidirectional Local-Global Interaction Guided GAN with Discriminator Gradient Gap Regularization for Bearing Fault Diagnosis with Unbalanced Datasets. IEEE Sensors Journal, 2025. doi: 10.1109/JSEN.2025.3538320.
6. Li L, Pan Z, Ma Y, Chen Z, Chen J, Wang Y. A new generative adversarial networks-based fault diagnosis framework: Learning a mapping to estimate fault. Neurocomputing, 2025; 622: 129288. doi: 10.1016/j.neucom.2024.129288.
7. Qin Z, Zhang Z, Wu Z, Zhang Q. Fault diagnosis method for rolling bearings under a small sample dataset based on improved WGAN-GP. Measurement, 2025: 118456. doi: 10.1016/j.measurement.2025.118456.
8. Liu Z, Zhang T, Huang Y, Mao X. Fault Diagnosis with Imbalanced Data: A Stable Sample Generation Approach Based on CWGAN-GP Model[C]//International Conference on Guidance, Navigation and Control. Singapore: Springer Nature Singapore, 2024: 582–590. doi: 10.1007/978-981-96-2228-3_54.
9. Wang X, Jiang H, Mu M, Dong Y. A trackable multi-domain collaborative generative adversarial network for rotating machinery fault diagnosis. Mechanical Systems and Signal Processing, 2025; 224: 111950. doi: 10.1016/j.ymssp.2024.111950.
10. Chu Z, Gu Z, Chen Y, Zhu D, Tang J. A fault diagnostic approach for underwater thrusters based on generative adversarial network. IEEE Transactions on Instrumentation and Measurement, 2024; 73: 1–14. doi: 10.1109/TIM.2024.3417591.
11. Han X, Cao Y, Hu P, Feng W. Multi-Modal and Multi-Condition Fault Diagnosis of Rotating Machinery via a Heterogeneous Graph Learning Framework. Information Fusion, 2025: 104106. doi: 10.1016/j.inffus.2025.104106.
12. Pham M T, Kim J M, Kim C H. Rolling bearing fault diagnosis based on improved GAN and 2-D representation of acoustic emission signals. IEEE Access, 2022; 10: 78056–78069. doi: 10.1109/ACCESS.2022.3193244.
13. Bai G, Sun W, Cao C, Wang D, Sun Q, Sun L. GAN-based bearing fault diagnosis method for short and imbalanced vibration signal. IEEE sensors journal, 2023; 24(2): 1894–1904. doi: 10.1109/JSEN.2023.3337278.
14. Yang J, Liu J, Xie J, Wang C, Ding T. Conditional GAN and 2-D CNN for bearing fault diagnosis with small samples. IEEE Transactions on Instrumentation and Measurement, 2021; 70: 1–12. doi: 10.1109/TIM.2021.3119135.
15. Gao H, Zhang X, Gao X, Li F, Han H. ICoT-GAN: Integrated convolutional transformer GAN for rolling bearings fault diagnosis under limited data condition. IEEE Transactions on Instrumentation and Measurement, 2023; 72: 1–14. doi: 10.1109/TIM.2023.3271729.
16. Jia Z, Yu B. A fault diagnosis method for rolling bearings of wind turbine generators based on MCGAN data enhancement. SN Applied Sciences, 2023; 5(10): 259. doi: 10.1007/s42452-023-05485-7.
17. Guo C, Potekhin V V, Li P, Kovalchuk E A, Lian J. MDFT-GAN: A Multi-Domain Feature Transformer GAN for Bearing Fault Diagnosis Under Limited and Imbalanced Data Conditions. Applied Sciences, 2025; 15(11): 6225. doi: 10.3390/app15116225.
18. Zhong H, Yu S, Trinh H, Yuan R, Lv Y, Wang Y. A time-saving fault diagnosis using simplified fast GAN and triple-type data transfer learning. Structural Health Monitoring, 2025; 24(2): 869–882. doi: 10.1177/14759217241241985.
19. Chen H, Wei J, Huang H, Yuan Y, Wang J. Review of imbalanced fault diagnosis technology based on generative adversarial networks. Journal of Computational Design and Engineering, 2024; 11(5): 99–124. doi: 10.1093/jcde/qwae075.
20. Wang Y, Sun G, Jin Q. Imbalanced sample fault diagnosis of rotating machinery using conditional variational auto-encoder generative adversarial network. Applied Soft Computing, 2020; 92: 106333. doi: 10.1016/j.asoc.2020.106333.
21. Ruan D, Song X, Gühmann C, Yan J. Collaborative optimization of CNN and GAN for bearing fault diagnosis under unbalanced datasets. Lubricants, 2021; 9(10): 105. doi: 10.3390/lubricants9100105.
22. Li W, Liu D, Li Y, Hou M, Liu J, Zhao Z, Guo A, Zhao H, Deng W. Fault diagnosis using variational autoencoder GAN and focal loss CNN under unbalanced data. Structural Health Monitoring, 2025; 24(3): 1859–1872. doi: 10.1177/14759217241254121.
23. Yang Z, Mao R, Ye L, Liu Y, Hu X, Li Y. VSC-ACGAN: bearing fault diagnosis model applied to imbalanced samples. Measurement Science and Technology, 2025; 36(3): 036212. doi: 10.1088/1361-6501/adb872.
24. Zhao Z, Sun S, Wang D, Xu W,. MCVAE-GAN: A novel diagnosis method for solving harmonic reducer fault signal scarcity and sample diversity problem. IEEE Transactions on Instrumentation and Measurement, 2024; 73: 1–10. doi: 10.1109/TIM.2024.3472781.
25. Wang X, Jiang H, Wu Z, Yang Q. Adaptive variational autoencoding generative adversarial networks for rolling bearing fault diagnosis. Advanced Engineering Informatics, 2023; 56: 102027. doi: 10.1016/j.aei.2023.102027.
26. Liu S, Jiang H, Wu Z, Li X. Data synthesis using deep feature enhanced generative adversarial networks for rolling bearing imbalanced fault diagnosis. Mechanical Systems and Signal Processing, 2022; 163: 108139. doi: 10.1016/j.ymssp.2021.108139.

27. Luo J, Huang J, Li H. A case study of conditional deep convolutional generative adversarial networks in machine fault diagnosis. Journal of Intelligent Manufacturing, 2021;32(2): 407–425. doi: 10.1007/s10845-020-01579-w.
28. Meng Z, Li Q, Sun D, Cao W, Fan F. An intelligent fault diagnosis method of small sample bearing based on improved auxiliary classification generative adversarial network. IEEE Sensors Journal, 2022; 22(20): 19543–19555. doi: 10.1109/JSEN.2022.3200691.
29. Viola J, Chen Y Q, Wang J. FaultFace: Deep convolutional generative adversarial network (DCGAN) based ball-bearing failure detection method. Information Sciences, 2021; 542: 195–211. doi: 10.1016/j.ins.2020.06.060.
30. Neupane D, Seok J. Bearing fault detection and diagnosis using case western reserve university dataset with deep learning approaches: A review. IEEE Access, 2020; 8: 93155–93178. doi: 10.1109/ACCESS.2020.2990528.
31. Zhang C, Wei S, Dong G, Zeng Y, Zhu G, Zhou X, Liu F. Time-domain sparsity-based bearing fault diagnosis methods using pulse signal-to-noise ratio. IEEE Transactions on Instrumentation and Measurement, 2024; 73: 1–4. doi: 10.1109/TIM.2024.3375978.
32. Zhang Q, Deng L. An intelligent fault diagnosis method of rolling bearings based on short-time Fourier transform and convolutional neural network. Journal of Failure Analysis and Prevention, 2023; 23(2): 795–811. doi: 10.1007/s11668-023-01616-9.
33. Wang J, Han B, Bao H, Wang M, Chu Z, Shen Y. Data augment method for machine fault diagnosis using conditional generative adversarial networks. Proceedings of the Institution of Mechanical Engineers, Part D: Journal of Automobile Engineering, 2020; 234(12): 2719–2727. doi: 10.1177/0954407020923258.
34. Gao X, Deng F, Yue X. Data augmentation in fault diagnosis based on the Wasserstein generative adversarial network with gradient penalty. Neurocomputing, 2020; 396: 487–494. doi: 10.1016/j.neucom.2018.10.109.
35. Li Y, Song Y, Jia L, Gao S, Li Q, Qiu M. Intelligent fault diagnosis by fusing domain adversarial training and maximum mean discrepancy via ensemble learning. IEEE Transactions on Industrial Informatics, 2020; 17(4): 2833–2841. doi: 10.1109/TII.2020.3008010.
36. Magadán L, Ruiz-Cárcel C, Granda J C, Suárez F J, Starr A. Explainable and interpretable bearing fault classification and diagnosis under limited data. Advanced Engineering Informatics, 2024; 62: 102909. doi: 10.1016/j.aei.2024.102909.